Composite Structures 153 (2016) 234–241

Contents lists available at ScienceDirect

Composite Structures

journal homepage: www.elsevier.com/locate/compstruct

A rational derivation of dynamic higher order equations for functionally graded micropolar plates

Hossein Abadikhah, Peter D. Folkow *

Department of Applied Mechanics, Chalmers University of Technology, SE-412 96 Göteborg, Sweden

ARTICLE INFO

Article history:
Received 20 May 2016
Accepted 23 May 2016
Available online 27 May 2016

Keywords:
Series expansion
Plate equation
Micropolar
Functionally graded
Eigenfrequency

ABSTRACT

The dynamics of functionally graded micropolar plates is considered. The derivation process is based on power series expansions in the thickness coordinate. Using the three-dimensional equations of motion for micropolar continuum, variationally consistent equations of motion and end boundary conditions are derived in a systematic fashion up to arbitrary order. Numerical results are presented for simply supported plates using different material distributions for both low and high order truncation orders. These results illustrate that the present approach renders benchmark solutions provided higher order truncations are used, and act as engineering plate equations using low order truncation.

1. Introduction

Functionally graded (FG) materials are composite materials made of two (or more) phases of material constituents, where the phase distribution varies continuously. The most used group of FG materials consists of ceramic and metal phases. Such materials were developed in the mid 1980s where the strength of the metal and the heat resistance of the ceramic made these materials well suited for high-temperature environments. FG materials also possess a number of further advantages compared to other inhomogeneous materials such as improved residual stress distribution, higher fracture toughness, and reduced stress intensity factors. Hence, FG materials are nowadays used in many different fields of engineering [1,2].

FG plates using classic elastic continuum theory have been studied extensively in recent decades. Among these, work on FG plates using three dimensional or higher order two dimensional theories are found in [3–9]. Several comprehensive surveys on various aspects of FG plate modeling have been reported [10–13].

In micropolar elasticity theory the classical continuum model is extended to properly deal with microscale effects which affects the mechanical response e.g. in granular or fibrous materials. In addition to the classical theory where three translational degrees of freedom are assigned to each material point, the micropolar theory adds three rotational degrees of freedom to each material point. This results in a so called couples stress tensor in addition to the regular stress tensor, where both these tensors are nonsymmetric in the general case. Among the different existing micropolar theories based on the Cosserat work [14], the version developed by Eringen [15] is perhaps the most popular. There are several work on micropolar plates adopting Eringen's theory [16–23], see also the review paper [24].

The present work on FG micropolar plates is an extension to the work on dynamic equations for homogeneous micropolar plates [23]. The method used renders a hierarchy of micropolar FG plate equations in a consistent and systematic fashion up to arbitrary order. The method is mainly based on the works on homogeneous plates that are isotropic [25], anisotropic [26] and piezoelectric [27], and has also been employed for functionally graded isotropic plates [3] adopting classic elastic continuum theory. The interest towards FG structures taking microscale effects into account has developed over the last few years. The majority of studies are based on the modified couple stress theory [28–32] and other alternative theories [33,34]. However, there are to our knowledge no work on FG plates using the more general micropolar theory, and thus this work may contribute to fill that gap.

The derivation process for developing plate equations for FG isotropic micropolar plates is here based on employing a systematic power series expansion approach using the three dimensional equations of motion for micropolar continuum. Displacement and micro-rotation fields, as well as material parameters, are expanded in a power series in the thickness coordinate of the plate. From these expanded fields, the stress and couple stress are obtained on power series form in terms of the expansion functions of the

* Corresponding author.
E-mail addresses: hossein.abadikhah@chalmers.se (H. Abadikhah), peter.folkow@chalmers.se (P.D. Folkow).

http://dx.doi.org/10.1016/j.compstruct.2016.05.090
0263-8223/

displacements and micro-rotations. Furthermore, by using the equations of motion for micropolar elasticity, recursion relations are constructed. These are used to express all expansion functions in terms of the lowest order expansion functions. Thus all fields can be expressed in these lowest order expansion functions without performing any truncations. Subsequently boundary conditions on the upper and lower surface of the plate are stated on power series form. These boundary conditions represent a set of scalar equations, written in terms of the lowest order expansion functions, and constitute the complete set of partial differential plate equations. Using variational calculus, the edge boundary conditions for each edge surface are obtained in an equally systematic manner. The resulting sets of plate equations may be truncated to any desired order. Numerical results are presented for simply supported plates where the material distribution is varying using a power law through the plate thickness. The results comprise eigenfrequencies and cross sectional fields using different truncation orders. The low order cases may be used as approximate engineering plate theories while the higher order theories act as benchmark theories converging to the exact 3D solution.

2. Theory of linear micropolar elasticity

Consider an isotropic micropolar continuum according to Eringen's theory [15]. The equations of balance of momentum and moment of momentum, written in cartesian coordinates, are expressed as

$$t_{kl,k} = \rho \ddot{u}_l, \tag{1}$$

$$m_{kl,k} + \epsilon_{lkm} t_{km} = \rho j_{lk} \ddot{\phi}_k, \tag{2}$$

in absence of body forces and body couples. Here t_{kl} is the stress tensor, m_{kl} is the couple stress tensor, u_l is the displacement vector, ϕ_k is the micro-rotation vector, ρ is the density, j_{lk} is the microinertia tensor and ϵ_{lkm} is the permutation symbol. Indices that follow a comma indicate partial differentiation. The surface tractions are defined in accordance to

$$t_l = t_{kl} n_k, \tag{3}$$

$$m_l = m_{kl} n_k, \tag{4}$$

where n_k is an outward pointing normal surface vector.

The micropolar strain tensors ε_{kl} and γ_{kl} are defined by

$$\varepsilon_{kl} = u_{l,k} + \epsilon_{lkm}\phi_m, \tag{5}$$

$$\gamma_{kl} = \phi_{k,l}. \tag{6}$$

These strain measures are related to the stress and couple stress tensors through the constitutive relations

$$t_{kl} = \lambda \varepsilon_{mm}\delta_{kl} + (\mu + \kappa)\varepsilon_{kl} + \mu \varepsilon_{lk}, \tag{7}$$

$$m_{kl} = \alpha \gamma_{mm}\delta_{kl} + \beta \gamma_{kl} + \gamma \gamma_{lk}, \tag{8}$$

where δ_{kl} is the Kronecker delta, λ and μ are Lamé parameters while α, β, γ and κ are micropolar elastic moduli. Consider from now on spin-isotropic materials where the microinertia reduces to a scalar quantity, $j_{kl} = j\delta_{kl}$.

3. Series expansion and recursion relations

A hierarchy of approximate equations for isotropic plates that are FG in the thickness direction is to be derived in a consistent manner based on governing equations for a micropolar continuum as described in Section 2. Consider a plate of thickness $2h$ using a cartesian coordinate system $\{x, y, z\}$, where the in plane x and y axes are along the middle plate plane at $z = 0$. The components of the displacement field and micro-rotation field are denoted $\{u_1, u_2, u_3\}$ and $\{\phi_1, \phi_2, \phi_3\}$ respectively. The derivation procedure of the plate equations is based on the assumption that each component of the displacement field and micro-rotation field can be expanded in a power series in the thickness coordinate z according to

$$u_l(x, y, z, t) = \sum_{n=0}^{\infty} z^n u_l^{(n)}(x, y, t), \tag{9}$$

$$\phi_l(x, y, z, t) = \sum_{n=0}^{\infty} z^n \phi_l^{(n)}(x, y, t), \tag{10}$$

for $l = 1, 2, 3$. As for the material parameters varying in the thickness direction, these are expanded in Taylor series [3] as

$$f(z) = \sum_{n=0}^{\infty} z^n f^{(n)}. \tag{11}$$

Here, f covers both traditional elastic parameters $\{\rho, \lambda, \mu\}$ and the micropolar parameters $\{\kappa, \alpha, \beta, \gamma, j\}$, see further discussions in Section 5.

By using the series expansions Eqs. (9)–(11) into the deformation relations Eqs. (5) and (6), the stress and couple stress expressions from the constitutive relations Eqs. (7) and (8) are written on power series form

$$t_{kl} = \sum_{n=0}^{\infty} z^n t_{kl}^{(n)}, \tag{12}$$

$$m_{kl} = \sum_{n=0}^{\infty} z^n m_{kl}^{(n)}. \tag{13}$$

Each power series term may thus be expressed in terms of displacements and rotations through

$$t_{kl}^{(n)} = \left[\lambda \bigstar L_j u_j\right]_n \delta_{kl} + \left[\mu \bigstar (L_l u_k + L_k u_l)\right]_n + \left[\kappa \bigstar (L_k u_l + \epsilon_{lkm}\phi_m)\right]_n, \tag{14}$$

$$m_{kl}^{(n)} = \left[\alpha \bigstar L_j \phi_j\right]_n \delta_{kl} + \left[\beta \bigstar L_l \phi_k\right]_n + \left[\gamma \bigstar L_k \phi_l\right]_n. \tag{15}$$

Here the product rule for power series are denoted

$$[a \bigstar b]_n = \sum_{i=0} n a^{(i)} b^{(n-i)}. \tag{16}$$

Moreover, operators L_k acting on the series expanded fields are introduced in order to simplify the expressions according to

$$L_k g_l^{(n)} = \begin{cases} \partial_x g_l^{(n)} & \text{if } k = 1, \\ \partial_y g_l^{(n)} & \text{if } k = 2, \\ (n+1) g_l^{(n+1)} & \text{if } k = 3, \end{cases} \tag{17}$$

where $g_l^{(n)}$ is any of the expansion fields in Eqs. (9)–(11). Hence L_k for $k = 3$ increases the index of $g_l^{(n)}$ and multiplies with the new index, in this case $n + 1$. Note the shorthand form ∂_x and ∂_y used to denote partial derivatives with respect to x and y.

Now that the material parameters, displacements, micro-rotations, stresses and couple stresses are all expressed on power series form according to Eqs. (9)–(13), these fields are to be used in the equations of motion, Eqs. (1) and (2). Collecting terms of equal power in z in the equations of motion results in recursion formulas for each displacement and micro-rotation field according to

$$\begin{aligned}(n+1)[(\mu+\kappa)\bigstar L_3 u_l]_{n+1} + (n+1)[(\lambda+\mu)\bigstar L_3 u_3]_{n+1}\delta_{3l} \\ = [\rho \bigstar \ddot{u}_l]_n - \left[(\mu+\kappa)\bigstar(\partial_x^2 + \partial_y^2)u_l\right]_n - L_l\left[\lambda \bigstar (\partial_x u_1 + \partial_y u_2)\right]_n \\ - \left[\mu \bigstar L_l(\partial_x u_1 + \partial_y u_2)\right]_n - (n+1)[\mu \bigstar L_l u_3]_{n+1}(1-\delta_{3l}) \\ - [\lambda \bigstar L_l L_3 u_3]_n (1-\delta_{3l}) - \epsilon_{ijk} L_j [\kappa \bigstar \phi_k]_n \delta_{li},\end{aligned} \tag{18}$$

$$(n+1)[\gamma\bigstar L_3\phi_l]_{n+1}+(n+1)[(\alpha+\beta)\bigstar L_3\phi_3]_{n+1}\delta_{3l}$$
$$=\left[J\bigstar\ddot{\phi}_l\right]_n-\left[\gamma\bigstar(\partial_x^2+\partial_y^2)\phi_l\right]_n-L_l\left[\alpha\bigstar(\partial_x\phi_1+\partial_y\phi_2)\right]_n$$
$$-\left[\beta\bigstar L_l(\partial_x\phi_1-\partial_y\phi_2)\right]_n-(n+1)[\beta\bigstar L_l\phi_3]_{n+1}(1-\delta_{3l})$$
$$-[\alpha\bigstar L_lL_3\phi_3]_n(1-\delta_{3l})-\epsilon_{ijk}\left[\kappa\bigstar L_ju_k\right]_n\delta_{li}+2[\kappa\bigstar\phi_l]_n, \tag{19}$$

for $l=1,2,3$ where $n=0,1,2\ldots$. Here $J=\rho j$ resulting in $J^{(n)}=[\rho\bigstar j]_n$. These recursion formulas are essential for the derivation of the plate equations since the number of expansion functions for each field can be reduced from an infinite amount to a finite amount. The highest order terms $u_l^{(n+2)}$ and $\phi_l^{(n+2)}$ present on the left hand sides of Eqs. (18) and (19), respectively, may thus be expressed in lower order terms. By using these formulas recursively it is possible to express all expansion functions $u_l^{(n)}$ and $\phi_l^{(n)}$ with $n=\{2,3,\ldots\}$ in terms of the twelve lowest order ones with $n=\{0,1\}$. Note that these coupled six recursion formulas do not involve any approximations since they stem from the equations of motion, Eqs. (1) and (2), and the power series expansion of the various fields. Furthermore, the power series have not been truncated which is crucial for the present method. Note that these recursion relations simplify to the ones in [23] for homogeneous micro plates, as well as to the ones in [3] for FG elastic plates without micro effects.

4. Plate equations and boundary conditions

This section covers the derivation of surface boundary conditions, that actually constitute the plate equations, and the edge boundary conditions.

4.1. Plate equations

On the surfaces at $z=\pm h$, either the tractions or the displacements and micro-rotation are to be prescribed. These given fields are denoted.

$\{T_l^{\pm},M_l^{\pm},U_l^{\pm},\Phi_l^{\pm}\}$ for $l=1,2,3$, where $\pm$ indicates the upper surface $z=h$ and the lower surface $z=-h$, respectively. Hence, for each l one field from $\{t_{3l},u_l\}$ and $\{m_{3l},\phi_l\}$ is to be prescribed, resulting in six boundary conditions on the upper and lower surfaces, respectively. In the case of prescribed tractions, the corresponding boundary conditions are obtained by truncating Eqs. (12) and (13) at an order $N>0$, which give

$$\sum_{n=0}^{N}(\pm h)^n t_{3l}^{(n)}(x,y,t)=T_l^{\pm}(x,y,t),\ \sum_{n=0}^{N}(\pm h)^n m_{3l}^{(n)}(x,y,t)=M_l^{\pm}(x,y,t). \tag{20}$$

Similarly boundary conditions for prescribed displacements and micro-rotations are obtained from Eqs. (9) and (10),

$$\sum_{n=0}^{N+1}(\pm h)^n u_l^{(n)}(x,y,t)=U_l^{\pm}(x,y,t),\ \sum_{n=0}^{N+1}(\pm h)^n \phi_l^{(n)}(x,y,t)=\Phi_l^{\pm}(x,y,t). \tag{21}$$

These surface boundary conditions are always fulfilled regardless of the expansion order N, which will be illustrated in the numerical examples Section 6.2. Note that the displacements and micro-rotations are truncated at a one order higher compared to the stresses. This is due to that stresses include spatial derivatives of one order higher than displacements and micro-rotations, therefore an extra term is added to these latter conditions in order to obtain consistent plate equations. Consequently, a total amount of twelve surface boundary conditions are to be chosen from Eqs. (20) and (21).

Using the recursion relations Eqs. (18) and (19) these boundary conditions may be written in terms of the twelve lowest order expansion functions $\{u_l^{(n)},\phi_l^{(n)}\}$ for $n=\{0,1\}$. Hereby each of the twelve boundary conditions given in Eqs. (20) and (21) contains spatial derivatives of order $N+1$ for $\{u_l^{(0)},\phi_l^{(0)}\}$ and spatial derivatives of order N for $\{u_l^{(1)},\phi_l^{(1)}\}$. This set of twelve surface boundary conditions constitutes the hyperbolic set of micropolar partial differential plate equations. The plate equation system is of differential order $12N$, which is seen by reducing the twelve equations to a single equation in any of the scalar fields $\{u_l^{(n)},\phi_l^{(n)}\}$ for $n=\{0,1\}$. Consequently $6N$ boundary conditions must be selected for each edge of the plate. It should be emphasized that it is not generally possible to obtain decoupled equations for symmetric and antisymmetric motions due to the inhomogeneous FG material distribution. These coupling effects make the solution process considerably more involved compared to the homogeneous micropolar plate case [23].

The presented set of plate equations may also be obtained from a more rigorous procedure using variational calculus in line with [23,35,36].

4.2. Edge conditions

Consider a rectangular plate where $-a\leqslant x\leqslant a$ and $-b\leqslant y\leqslant b$. At each edge $x=\pm a$ one field from each pair $\{t_{1l},u_l\}$ and $\{m_{1l},\phi_l\}$ for $l=1,2,3$ is to be prescribed for all $z\in[-h,h]$. Similarly, at $y=\pm b$ one field from each pair $\{t_{2l},u_l\}$ and $\{m_{2l},\phi_l\}$ should be given. The given fields are denoted $\{T_l^{\{\pm a,\pm b\}},U_l^{\{\pm a,\pm b\}}\}$ and $\{M_l^{\{\pm a,\pm b\}},\Phi_l^{\{\pm a,\pm b\}}\}$ for each edge. These prescribed edge boundary fields may be time dependent as well as having varying properties over the thickness and along each edge. The $6N$ boundary conditions at each edge are to be derived in a systematic manner by adopting variational calculus. Since all boundary conditions are constructed in the same manner, the procedure is only presented explicitly for prescribed tractions at $x=a$, that is T_l^{+a}. Using generalized Hamilton's principle [23,26,35,36], the variationally consistent edge boundary conditions adopting Eq. (12) are expressed as

$$\int_{-h}^{h}\left(T_l^{+a}(y,z,t)-\sum_{n=0}^{N-1}z^n t_{1l}^{(n)}(a,y,t)\right)z^k dz=0,\quad k=0,1,\ldots,N-1, \tag{22}$$

for $l=1,2,3$. The N integrals in Eq. (22) for each l constitute a system of equations which solution renders the N terms $t_{1l}^{(n)}(a,y,t)$ for $n=0,1,\ldots,N-1$. This representation of the boundary condition in power series form is identical to the expansion of the given functions T_l^{+a} in terms of Legendre polynomials $P_n(z/h)$ of order $N-1$, i.e.

$$T_l^{+a}(y,z,t)\approx\sum_{n=0}^{N-1}a_n(y,t)P_n(z/h)=\sum_{n=0}^{N-1}z^n T_l^{+a^{(n)}}(y,t), \tag{23}$$

hence $t_{1l}^{(n)}(a,y,t)=T_l^{+a^{(n)}}(y,t)$. Note that the stress free case $T_l^{+a}=0$ results in $t_{1l}^{(n)}=0$ for all n at the edge. By using Eq. (14) each edge boundary stress term $t_{1l}^{(n)}(a,y,t)$ is expressed in terms of displacements and micro-rotations. Adopting the recursions formulas Eqs. (18) and (19), the boundary stresses are written as partial differential equations in terms of the lowest order fields $\{u_l^{(n)},\phi_l^{(n)}\}$ for $n=\{0,1\}$.

It should be emphasized that these sets of plate differential equations, together with pertinent edge boundary conditions, constitute a hierarchy of variationally consistent plates equations that may be truncated to arbitrary order.

5. Properties of FG materials

There are rather few investigations presented in the literature where micropolar material parameters are obtained

experimentally. Material data obtained from eigenfrequency analyses are presented in [37] for aluminum as well as for an epoxy matrix containing aluminum spheres. The first single material case uses measured experimental data, while the second two-phase material case uses numerical data [15,38].

For a FG plate the material parameters are to vary continuously over the thickness. Consider a plate where the top $z=h$ (subscript t) consists of pure aluminum, while the bottom $z=-h$ (subscript b) consists of epoxy containing randomly distributed aluminum particles. Consequently, the amount of aluminum decreases continuously from the top to the bottom of the plate. From [37] the material parameters for aluminum at the top are $\lambda_t = 51.704$ GPa, $\mu_t = 26.635$ GPa, $\rho_t = 2800$ kg/m^3, $j_t = 0.325\times 10^{-7}$ m^2, $\kappa_t = 1.3155\times 10^{-5}$ GPa, $\alpha_t = 1.2355$ kN, $\beta_t = 0.1585$ kN, $\gamma_t = 0.59664$ kN while for the epoxy matrix with aluminum particles at the bottom one has $\lambda_b = 7.586$ GPa, $\mu_b = 1.896$ GPa, $\rho_b = 2192$ kg/m^3, $j_b = 1.96\times 10^{-7}$ m^2, $\kappa_b = 1.3234\times 10^{-4}$ GPa, $\alpha_b = 83.255$ N, $\beta_b = 0.1028$ kN, $\gamma_b = 3.3349$ kN. Note that these values cause the stress tensor in Eq. (7) to be close to symmetric due to small value of the ratio κ/μ.

There are different ways to model the variation of the materials over the thickness, e.g. adopting a power law or an exponential law. Here consider the often used power law where the volume fraction of the bottom material varies as

$$V_b(z) = ((h-z)/2h)^p. \tag{24}$$

Note that the volume fraction law follows $V_b + V_t = 1$, and the power index p is a positive number.

There are various methods to model the effective material properties in FG materials. Among these the rule of mixture (Voigt model) is perhaps the simplest, while other theories such as the Mori–Tanaka model and the self-consistent model take microstructural aspects into account, see discussion in [2,39]. In the Voigt model the various material properties (denoted by Q) are assumed to be proportional to the volume ratio according to

$$Q(z) = Q_b V_b(z) + Q_t V_t(z). \tag{25}$$

This model is generally used for the effective density, which is also the case in the present work. The Voigt model is also often used for the elastic Lamé parameters λ and μ, although more refined theories such as the Mori–Tanaka model or the self-consistent model may be adopted. The Mori–Tanaka model [40] is mainly used for two-phase materials where there is a clearly defined continuous matrix with discontinuous particles, whereas the more involved self-consistent model is mainly used for two-phase materials where each phase has an interconnected skeletal microstructure [11]. Here the Mori–Tanaka model is chosen due to the distribution of separate aluminum particles in the lower part of the plate. Hence, the Lamé parameters are obtained through

$$\frac{K(z)-K_t}{K_b-K_t} = \frac{V_b(z)}{1+V_t(z)(3(K_b-K_t)/(3K_t+\mu_t))}, \tag{26}$$

$$\frac{\mu(z)-\mu_t}{\mu_b-\mu_t} = \frac{V_b(z)}{1+V_t(z)(\mu_b-\mu_t)/(\mu_t+f)}, \tag{27}$$

where

$$f = \frac{\mu_t(9K_t+8\mu_t)}{6(K_t+2\mu_t)}. \tag{28}$$

Here $K=\lambda+2\mu/3$ is the bulk modulus. As for the effective micro parameters $\{\kappa,\alpha,\beta,\gamma,j\}$, there are to our knowledge no investigations on how to model these for FG materials. Here, they are supposed to follow the Voigt estimate Eq. (25).

6. Numerical results

The object for the numerical results is to illustrate the accuracy of the present partial differential equations for FG micropolar plates; both for low and high order sets. The low order cases may be used as approximate engineering plate theories while the higher order theories act as benchmark theories converging to the exact 3D solution. Although any type of surface boundary conditions may be studied, consider only the case with free upper and lower plate surfaces. Consequently, the surface boundary conditions are obtained from Eq. (20) with $T_l^{\pm}=0$ and $M_l^{\pm}=0$. For the numerical process, it is convenient to express these twelve conditions in terms of sums and differences [23]. Hence, the resulting equations become

$$\sum_{n\ \text{even}}^{N} h^n p_{3l}^{(n)} = 0, \quad \sum_{n\ \text{odd}}^{N} h^n p_{3l}^{(n)} = 0, \tag{29}$$

for $l=1,2,3$ where p_{3l} stands for both the stresses t_{3l} and the couple stresses m_{3l}.

As for the edge boundary conditions, consider mixed conditions (simply supported) using the notation in Section 4.2

$$\begin{aligned} &U_2^{\pm a}=0,\quad U_3^{\pm a}=0,\quad T_1^{\pm a}=0,\quad \Phi_1^{\pm a}=0,\quad M_2^{\pm a}=0,\quad M_3^{\pm a}=0,\\ &U_1^{\pm b}=0,\quad U_3^{\pm b}=0,\quad T_2^{\pm b}=0,\quad \Phi_2^{\pm b}=0,\quad M_1^{\pm b}=0,\quad M_3^{\pm b}=0. \end{aligned} \tag{30}$$

Hence, each series expansion term becomes

$$\begin{aligned} &u_2^{(n)}=0,\quad u_3^{(n)}=0,\quad t_{11}^{(n)}=0,\quad \phi_1^{(n)}=0,\quad m_{12}^{(n)}=0,\quad m_{13}^{(n)}=0,\quad x=\pm a,\\ &u_1^{(n)}=0,\quad u_3^{(n)}=0,\quad t_{22}^{(n)}=0,\quad \phi_2^{(n)}=0,\quad m_{21}^{(n)}=0,\quad m_{23}^{(n)}=0,\quad y=\pm b, \end{aligned} \tag{31}$$

for $n=0,1,2\ldots$.

The presented results below are for eigenfrequencies for square plates as well as mode shapes and stress distributions over the cross section.

6.1. Eigenfrequencies

In this section, eigenfrequencies for a square plate $a=b$ are calculated for two different plate thicknesses: $a/h=20$ and $a/h=8$. In order to study the influence from the material distribution, different power indexes p from Eq. (24) are considered. For each case the three lowest eigenfrequencies ω_{mn} are calculated using different truncation orders, where m and n refer to the mode numbers in the x and y directions, respectively. These eigenfrequencies are mainly of antisymmetric character involving flexural motion. For convenience, introduce the non dimensional frequency $\Omega_{mn}=\omega_{mn}h/c_E$, where the velocity c_E for the bottom epoxy/aluminum material is defined as $c_E=\sqrt{E_b/\rho_b}$ using the relation between the Young and Lamé parameters $E_b=\mu_b(3\lambda_b+2\mu_b)/(\lambda_b+\mu_b)$.

The results are given in Tables 1 and 2 for different truncation orders. Here the case $N=1$ is disregarded as it captures the modes that are of predominately symmetric behavior resulting in considerably higher eigenfrequencies [26,27]. Note that higher eigenfrequencies are obtained for the less slender plate as expected. Moreover the eigenfrequencies become higher by increasing the power index p, as this results in higher amount of the aluminum phase. For comparison, the exact eigenfrequencies for the single aluminum phase (corresponds to $p\to\infty$) and for the even distribution of the epoxy/aluminum phase (corresponds to $p=0$) are given in Table 3.

As for the different truncation orders in Tables 1 and 2, it is seen that the series method converges reasonably rapidly in most cases.

Table 1
Eigenfrequencies Ω_{mn} for a quadratic plate with $a/h = 20$ using different truncation orders.

p	mn	$N = 2$	$N = 3$	$N = 4$	$N = 6$	$N = 10$	$N = 25$	$N = 50$
1	11	0.019822	0.013417	0.015348	0.014925	0.014899	0.014898	0.014898
	12	0.048696	0.033164	0.037962	0.036899	0.036831	0.036829	0.036829
	22	0.076623	0.052501	0.060117	0.058404	0.058294	0.058291	0.058291
2	11	0.024394	0.017173	0.016703	0.016776	0.016855	0.016852	0.016852
	12	0.059935	0.042431	0.041381	0.041513	0.041710	0.041703	0.041702
	22	0.094319	0.067135	0.065629	0.065764	0.066079	0.066067	0.066067
3	11	0.026845	0.020354	0.016081	0.018402	0.018032	0.018004	0.018004
	12	0.065958	0.050225	0.039895	0.045531	0.044631	0.044564	0.044563
	22	0.10380	0.079362	0.063356	0.072120	0.070718	0.070613	0.070611
5	11	0.028818	0.023500	0.017926	0.018851	0.019325	0.019428	0.019427
	12	0.070803	0.057905	0.044433	0.046659	0.047825	0.048077	0.048074
	22	0.11142	0.091367	0.070503	0.073933	0.075776	0.076168	0.076162

Table 2
Eigenfrequencies Ω_{mn} for a quadratic plate with $a/h = 8$ using different truncation orders.

p	mn	$N = 2$	$N = 3$	$N = 4$	$N = 6$	$N = 10$	$N = 25$	$N = 50$
1	11	0.11692	0.080781	0.092557	0.089857	0.089683	0.089678	0.089678
	12	0.26837	0.19078	0.21897	0.21208	0.21161	0.21159	0.21159
	22	0.40022	0.29085	0.33408	0.32301	0.32219	0.32217	0.32217
2	11	0.14394	0.10322	0.10125	0.10130	0.10179	0.10177	0.10177
	12	0.33050	0.24312	0.24120	0.23998	0.24115	0.24111	0.24111
	22	0.49300	0.36979	0.36993	0.36644	0.36825	0.36819	0.36819
3	11	0.15840	0.12180	0.097928	0.11106	0.10895	0.10880	0.10879
	12	0.36370	0.28493	0.23487	0.26284	0.25828	0.25794	0.25793
	22	0.54255	0.43098	0.36220	0.40092	0.39453	0.39403	0.39403
5	11	0.17003	0.13994	0.10884	0.11390	0.11673	0.11732	0.11731
	12	0.39034	0.32499	0.25986	0.26992	0.27655	0.27781	0.27779
	22	0.58224	0.48860	0.39929	0.41205	0.42219	0.42394	0.42391

Table 3
Exact eigenfrequencies Ω_{mn} for a quadratic plate of either aluminum or epoxy/aluminum.

Material	mn	$a/h = 20$	$a/h = 8$
Al	11	0.024171	0.14463
	12	0.059647	0.33808
	22	0.094248	0.51080
Ep/Al	11	0.0077182	0.045931
	12	0.018988	0.10686
	22	0.029980	0.16091

As expected, the rate of convergence decreases as the power index increases. However, it is a bit surprising that the accuracies of the different truncation orders are not much affected by the plate thickness or the mode numbers; at least not for the cases studied here. Although the accuracies generally increase when raising the truncation orders, the case for $p = 2$ when $a/h = 8$ is contradicting this. Here the case $N = 3$ is superior to both the cases $N = 4$ and $N = 6$ when $m = n = 2$, albeit the differences are small. The reason for this is unclear to us, in particular since this behavior does not appear for the other power indexes when $a/h = 8$ or in any cases for the thinner plate.

By studying the higher truncation orders more in detail, it is seen that the results for the highest presented order ($N = 50$) seem to be accurate to all the given figures. Hence, these eigenfrequencies may be used as benchmark results to the exact 3D theory [3]. It should be stressed that the present derivation process, when applied to other materials presented in the literature, render consistent numerical results for homogeneous micropolar plates [35] as well as for functionally graded elastic plates [3].

6.2. Eigenmodes

In order to further illustrate the differences between the truncation orders, various plots on mode shapes and stress distributions are compared. Consider only the case $p = 3$ for the fundamental frequency Ω_{11} for $a/h = 8$. Here the differences among the low order truncations are reasonably perceivable in several of the fields. The eigenmode shapes are plotted as functions of the non dimensional thickness coordinate z/h in the middle area of the plate $x = y = 0$, where the normalization is such that the vertical displacement u_3 equals unity at $z = 0$.

Fig. 1 shows the displacements in the x- and z-directions, u_1 and u_3, respectively. It is clearly seen that the fundamental mode is predominately flexural, as the u_1 field is close to antisymmetric and the u_3 field is close to symmetric with respect to z. This behavior is most visible for the $N = 2$ case, where the low order expansion order does not capture the inhomogeneous effects properly. The results from $N = 3$ and $N = 4$ are almost overlapping, while the $N = 10$ curve is indistinguishable from the high order benchmark curve $N = 50$. This latter conformity for the higher modes are visible in most cases presented below.

Next consider the normal stress t_{11} in Fig. 2(a). Here the differences among the truncation orders are more pronounced when compared to the displacements and the eigenfrequencies. Note that the antisymmetric behavior that would appear for a homogeneous plate is disrupted due to the FG material distribution, even for the $N = 2$ case. The shear stress t_{12} is illustrated in Fig. 2(b) where the stress distribution variation resembles t_{11}. Fig. 3 illustrates the normal stress t_{33} and the shear stress t_{31}. Here the differences among the various truncation orders are more easily visible, although the absolute values and the variation of the stresses over the thickness are much lower than for t_{11}. For $N = 2$ the shear

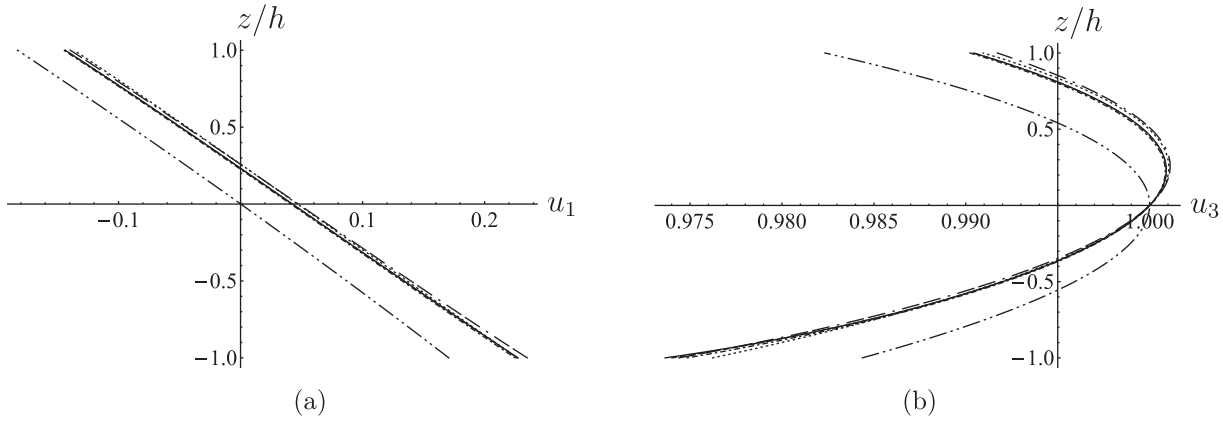

Fig. 1. Displacement in x-direction u_1 (a) and z-direction u_3 (b) for the first mode with $p = 3$: —— $N = 50$, - - - $N = 10$, - . - $N = 6$, – –.– – $N = 4$, ⋯ $N = 3$, –..– $N = 2$.

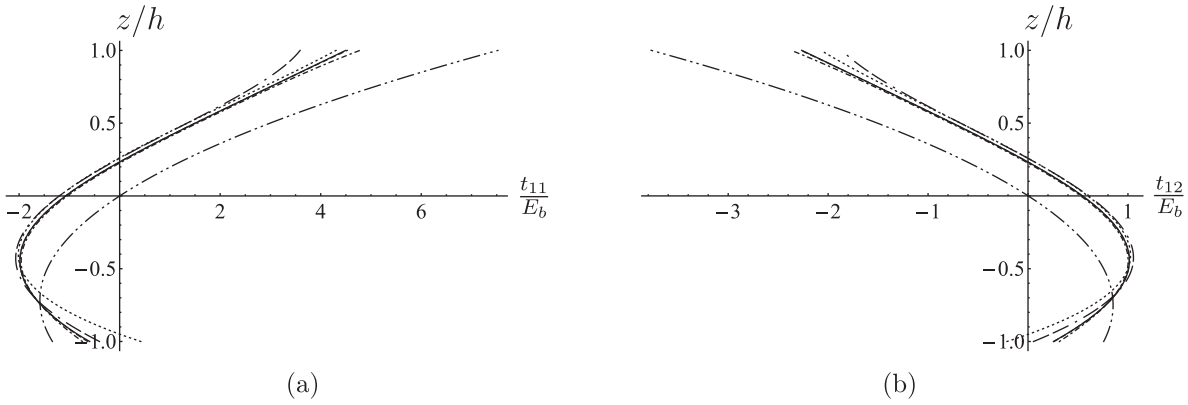

Fig. 2. Normal stress in x-direction t_{11} (a) and shear stress t_{12} (b) for the fundamental eigenfrequency, $p = 3$: —— $N = 50$, - - - $N = 10$, -.- $N = 6$, – –.– – $N = 4$, ⋯ $N = 3$, –..– $N = 2$.

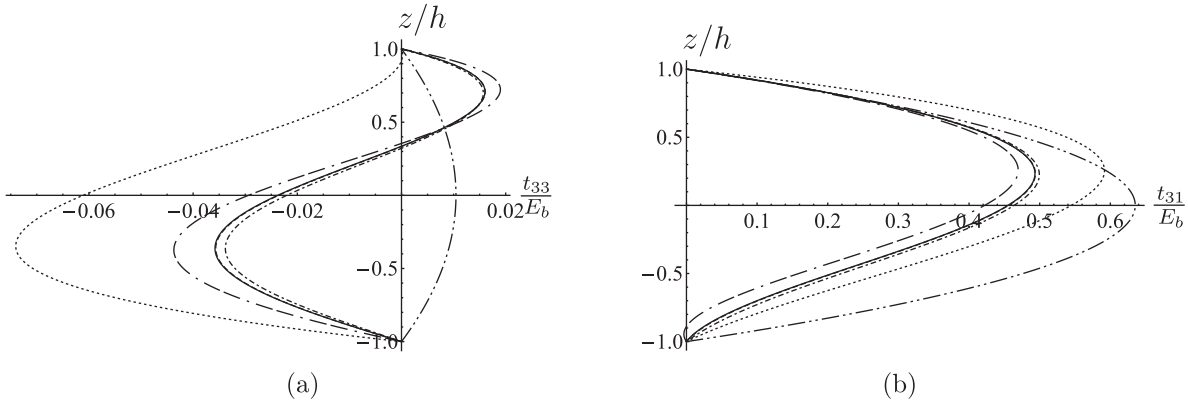

Fig. 3. Normal stress in z-direction t_{33} (a) and shear stress t_{31} (b) for the fundamental eigenfrequency, $p = 3$: —— $N = 50$, - - - $N = 10$, -.- $N = 6$, – –.– – $N = 4$, ⋯ $N = 3$, –..– $N = 2$.

stress t_{31} in Fig. 3(b) is almost symmetric as for a non-varying material. However, the second order polynomial used in the $N = 2$ case for the normal stress t_{33} in Fig. 3(a) does not capture the higher order variation over the thickness properly. Note that all truncation orders fulfill the stress free boundary condition at the free surfaces $z = \pm h$ as illustrated in Fig. 3(a) and (b). The field t_{13} is similar to t_{31}, and all the fields related to the y direction $(u_2, t_{22}, t_{21}, t_{23}, t_{32})$ have field distributions resembling the corresponding ones presented above due to the xy symmetry of the problem. Hence, these fields are not illustrated here.

As for the micro effects, Fig. 4(a) illustrates the micro rotation ϕ_1. It is seen that the $N = 2$ case is almost constant over the thickness, while the other truncations show a slight variation in the micro rotational field. The behavior is similar for ϕ_2 while ϕ_3 is identical to zero since there is no micro rotation around the z-axis for this mode. The normal couple stress m_{11} in Fig. 4(b) shows little variation among the truncation orders as only $N = 2$ differs in a visible manner. The field m_{22} varies in a similar way while m_{33} is identical to zero due to its relation to ϕ_3 and the xy symmetry of the problem. The field variations of m_{12} and m_{21}

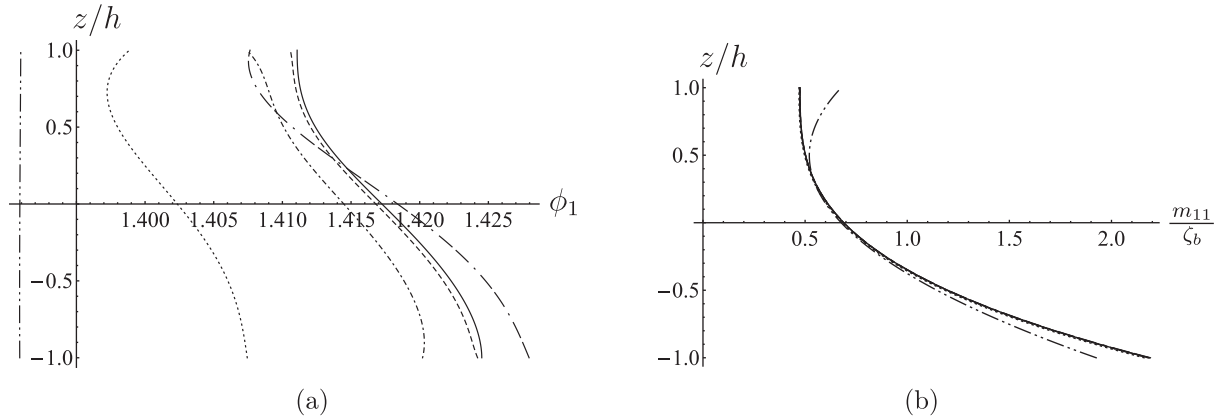

Fig. 4. Micro-rotation in x-direction ϕ_1 (a) and normal couple stress in x-direction m_{11} (b) for the first mode with $p = 3$: —— $N = 50$, - - - $N = 10$, -.- $N = 6$, – –.– – $N = 4, \cdots N = 3$, –..– $N = 2$.

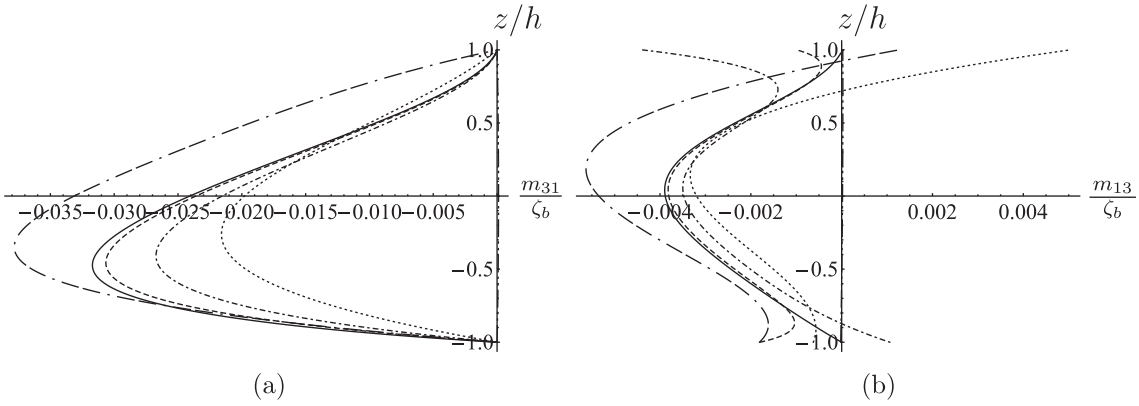

Fig. 5. Shear couple stresses m_{31} (a) and m_{13} (b) for the first mode with $p = 3$: —— $N = 50$, - - - $N = 10$, -.- $N = 6$, – –.– – $N = 4, \cdots N = 3$, –..– $N = 2$.

resembles m_{11} and m_{22}, respectively. These fields are not presented here. Note that $\zeta_b = \alpha_b + \beta_b + \gamma_b$.

As for the couple stresses m_{13} and m_{31} there are more mutual discrepancies as illustrated in Fig. 5. Note that both stress fields should be zero at the top and bottom surfaces: m_{31} due to the stated stress free boundary condition and m_{13} from Eq. (8) using that ϕ_3 is identical to zero. For each truncation order the field m_{31} at these surfaces is automatically fulfilled due to the stated boundary condition, while the field m_{13} at these surfaces is obtained using the micro rotation ϕ_1 calculated from the complete process described in the previous sections. In this latter case, many terms are needed in order to get the correct behavior close to these surfaces as illustrated in Fig. 5(b). Note that the field for $N = 2$ is close to zero over the thickness in both cases. The corresponding fields m_{23} and m_{32} have similar field variations not illustrated here.

7. Conclusion

This work presents a systematic approach for deriving sets of partial differential equations and pertinent end boundary conditions for FG micropolar plates. The method used is based on a power series expansion approach which result in variationally consistent plate equations of various truncation orders. The lower order expansions may be used as engineering plate equations while the higher order theories may act as benchmark solutions. Numerical examples are presented for a plate made of aluminum and epoxy. Using a power law distribution of the material volume fraction, the variation of material parameters are based on the Voigt and the Mori–Tanaka models.

Numerical results are presented for square plates with simply supported edges for different power indexes using both low order truncations as well as high order truncations. For the eigenfrequency examples studied herein, modest to high order truncations are in several cases required to render results that are of adequate accuracy. This differs to the homogeneous micropolar plate case studied in [23] where low to modest order truncations are sufficient. Due to the more involved FG material in the present work, higher order truncations are needed and presented to render benchmark solutions. As for the mode shapes and stress distributions for the first mode, the variation over the plate thickness and between the truncation orders are more pronounced for the present FG case compared to the homogeneous case in [23]. By performing comparisons to FG isotropic plates adopting classic elastic continuum theory as studied in [3], both systems show similarities regarding the rate of convergence for the eigenfrequencies using different order truncations, as well as the cross sectional distribution of the mode shapes.

References

[1] Birman V, Byrd LW. Modeling and analysis of functionally graded materials and structures. Appl Mech Rev 2007;60:195–216.
[2] Shen HS. Functionally graded materials: nonlinear analysis of plates and shells. CRC Press; 2009.
[3] Vel SS, Batra RC. Three-dimensional exact solution for the vibration of functionally graded rectangular plates. J Sound Vib 2004;272:703–30.

[4] Roque CMC, Ferreira AJM, Jorge RMN. A radial basis function approach for the free vibration analysis of functionally graded plates using a refined theory. J Sound Vib 2007;300:1048–70.
[5] Uymaz B, Aydogdu M. Three-dimensional vibration analyses of functionally graded plates under various boundary conditions. J Reinf Plast Compos 2007;26:1847–63.
[6] Matsunaga H. Free vibration stability of functionally graded plates according to a 2-D higher-order deformation theory. Comput Struct 2008;82:499–512.
[7] Reddy JN, Cheng ZQ. Frequency of functionally graded plates with three-dimensional asymptotic approach. J Eng Mech 2003;129:896–900.
[8] Jin G, Su Z, Ye T, Gao S. Three-dimensional exact solution for the free vibration of arbitrarily thick functionally graded rectangular plates with general boundary conditions. Compos Struct 2014;108:565–77.
[9] Reddy KSK, Kant T. Three-dimensional elasticity solution for free vibrations of exponentially graded plates. J Eng Mech 2014;140:04014047.
[10] Liew KM, Zhao X, Ferreira AJM. A review of meshless methods for laminated and functionally graded plates and shells. Compos Struct 2011;93:2031–41.
[11] Jha DK, Kant T, Singh RK. A critical review of recent research on functionally graded plates. Compos Struct 2013;96:833–49.
[12] Thai H-T, Kim S-E. A review of theories for the modeling analysis of functionally graded plates and shells. Compos Struct 2015;128:70–86.
[13] Swaminathan K, Naveenkumar DT, Zenkour AM, Carrera E. Stress, vibration and buckling analyses of FGM plates – a state-of-the-art review. Compos Struct 2015;120:10–31.
[14] Cosserat EF. Théorie des Corps Déformables. A Herman et Fils Paris; 1906.
[15] Eringen AC. Microcontinuum field theories. Foundations solids, vol. I. Springer; 1999.
[16] Eringen AC. Theory of micropolar plate. Z Angew Math Phys 1967;18:12–30.
[17] Green AE, Naghdi PM. Micropolar director theories of plates. Q J Mech Appl Math 1967;20:183–99.
[18] Wang F-Y. On the solutions of Eringen's micropolar plate equations and of other approximate equations. Int J Eng Sci 1990;28:919–25.
[19] Erbay HA. An asymptotic theory of thin micropolar plates. Int J Eng Sci 2000;38:1497–516.
[20] Altenbach H, Eremeyev VA. On the linear theory of micropolar plates. Z Angew Math Mech 2009;89:242–56.
[21] Sargsyan SH, Sargsyan AH. Dynamic model of micropolar elastic thin plates with independent fields of displacements and rotations. J Sound Vib 2014;333:4354–75.
[22] Steinberg L, Kvasov R. Analytical modeling of vibration of micropolar plates. Appl Math 2015;6:817–36.
[23] Abadikhah H, Folkow PD. A hierarchy of dynamic equations for micropolar plates. J Sound Vib 2015;357:427–36.
[24] Altenbach J, Altenbach H, Eremeyev VA. On generalized Cosserat-type theories of plates shells: a short review bibliography. Arch Appl Mech 2010;80:73–92.
[25] Boström A, Johansson G, Olsson P. On the rational derivation of a hierarchy of dynamic equations for a homogeneous isotropic elastic plate. Int J Solids Struct 2001;38:2487–501.
[26] Mauritsson K, Folkow PD, Boström A. Dynamic equations for a fully anisotropic elastic plate. J Sound Vib 2011;330:2640–54.
[27] Mauritsson K, Folkow PD. Dynamic equations for a fully anisotropic piezoelectric rectangular plate. Comput Struct 2015;153:112–25.
[28] Reddy JN, Kim J. A nonlinear modified couple stress-based third-order theory of functionally graded plates. Compos Struct 2012;94:1128–43.
[29] Thai H-T, Choi DH. Size-dependent functionally graded Kirchhoff and Mindlin plate models based on a modified couple stress theory. Compos Struct 2013;95:142–53.
[30] Lou J, He L, Du J. A unified higher order plate theory for functionally graded microplates based on the modified couple stress theory. Compos Struct 2015;133:1036–47.
[31] Salehipour H, Nahvi H, Shahidi AR. Exact closed-form free vibration analysis for functionally graded micro/nano plates based on modified couple stress and three-dimensional elasticity theories. Compos Struct 2015;124:283–91.
[32] He L, Lou J, Zhang E, Wang Y, Bai Y. A size-dependent four variable refined plate model for functionally graded microplates based on modified couple stress theory. Compos Struct 2015;130:107–15.
[33] Sahmani S, Ansari R. On the free vibration response of functionally graded higher-order shear deformable microplates based on the strain gradient elasticity theory. Compos Struct 2013;695:430–42.
[34] Jędrysiak J. Modelling of dynamic behaviour of microstructured thin functionally graded plates. Thin-Wall Struct 2013;71:102–7.
[35] Abadikhah H, Folkow PD. A hierarchy of dynamic equations for solid isotropic circular cylinders. Wave Motion 2013;51:206–21.
[36] Folkow PD, Mauritsson K. Dynamic higher-order equations for finite rods. Q J Mech Appl Math 2010;63:1–22.
[37] Kiris A, Inan E. On the identification of microstretch elastic moduli of materials by using vibration data on plates. Int J Eng Sci 2008;46:585–97.
[38] Gauthier RD. Experimental investigations of micropolar media mechanics of micropolar media. Singapore: World Scientific; 1982. p. 395–63.
[39] Akbarzadeh AH, Abedini A, Chen ZT. Effect of micromechanical models on structural responses of functionally graded plates. Compos Struct 2015;119:598–609.
[40] Mori T, Tanaka T. Average stress in matrix and average elastic energy of materials with misfitting inclusions. Acta Metall 1973;21:571–4.